ACS Sustainable Chemistry & Engineering

Research Article

pubs.acs.org/journal/ascecg

A Mechanistic Investigation of Acid-Catalyzed Cleavage of Aryl-Ether Linkages: Implications for Lignin Depolymerization in Acidic Environments

Matthew R. Sturgeon,[†,‡,⊥] Seonah Kim,[†,‡,⊥] Kelsey Lawrence,[†] Robert S. Paton,[§] Stephen C. Chmely,[‡,¶] Mark Nimlos,[†] Thomas D. Foust,[†,‡] and Gregg T. Beckham*[,†,‡,∥]

[†]National Advanced Biofuels Consortium, National Renewable Energy Laboratory, Golden, Colorado 80401, United States

[‡]National Bioenergy Center, National Renewable Energy Laboratory, Golden, Colorado 80401, United States

[§]Chemistry Research Laboratory, University of Oxford, 12 Mansfield Road, Oxford OX1 3TA, United Kingdom

[∥]Department of Chemical Engineering, Colorado School of Mines, Golden, Colorado 80401, United States

Supporting Information

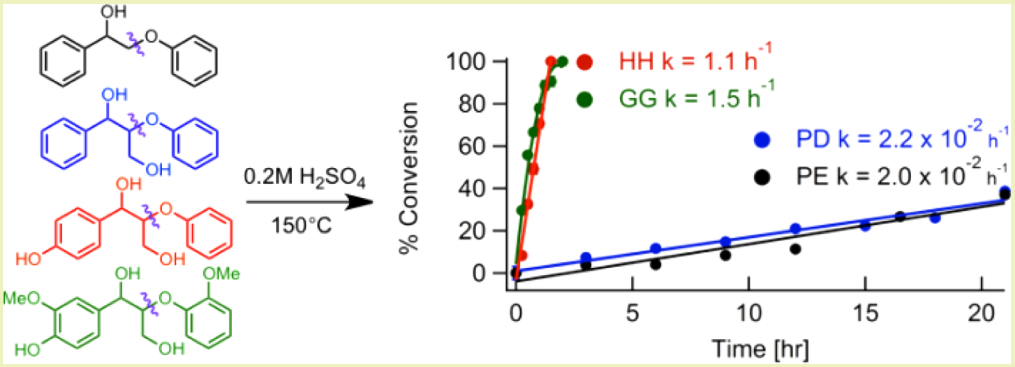

ABSTRACT: Acid catalysis has long been used to depolymerize plant cell wall polysaccharides, and the mechanisms by which acid affects carbohydrates have been extensively studied. Lignin depolymerization, however, is not as well understood, primarily due to the heterogeneity and reactivity of lignin. We present an experimental and theoretical study of acid-catalyzed cleavage of two non-phenolic and two phenolic dimers that exhibit the β-O-4 ether linkage, the most common intermonomer bond in lignin. This work demonstrates that the rate of acid-catalyzed β-O-4 cleavage in dimers exhibiting a phenolic hydroxyl group is 2 orders of magnitude faster than in non-phenolic dimers. The experiments suggest that the major product distribution is similar for all model compounds, but a stable phenyl-dihydrobenzofuran species is observed in the acidolysis of two of the γ-carbinol containing model compounds. The presence of a methoxy substituent, commonly found in native lignin, prevents the formation of this intermediate. Reaction pathways were examined with quantum mechanical calculations, which aid in explaining the substantial differences in reactivity. Moreover, we use a radical scavenger to show that the commonly proposed homolytic cleavage pathway of phenolic β-O-4 linkages is unlikely in acidolysis conditions. Overall, this study explains the disparity between rates of β-O-4 cleavage seen in model compound experiments and acid pretreatment of biomass, and implies that depolymerization of lignin during acid-catalyzed pretreatment or fractionation will proceed via a heterolytic, unzipping mechanism wherein β-O-4 linkages are cleaved from the phenolic ends of branched, polymer chains inward toward the core of the polymer.

KEYWORDS: *Density functional theory, Biofuels, β-O-4, Ether bond*

INTRODUCTION

Lignocellulosic plant biomass represents the largest terrestrial renewable carbon source on Earth. As such, significant efforts have been undertaken to utilize biomass for the large-scale production of fuels and chemicals in an effort to reduce dependence on nonrenewable fossil fuels.[1−3] Plant cell walls are primarily comprised of carbohydrate polymers in the form of cellulose, hemicellulose, and pectin as well as the heterogeneous, alkyl-aromatic polymer, lignin. To date, most research efforts for biomass conversion have focused on development of methods to utilize the carbohydrate fraction of plant biomass via fermentation to ethanol[4] or more recently via biological or chemical pathways to higher alcohols, hydrogen, hydrocarbons, or high-value chemicals.[5−9] Routes from carbohydrates to fuels

Received: September 30, 2013
Revised: November 6, 2013
Published: November 11, 2013

or chemicals typically slate the lignin fraction of biomass for combustion to produce heat and power,[1,10] and thus lignin utilization for nonheat and power products has received less attention.[11] However, lignin represents up to 30% of some biomass feedstocks, and thus understanding the mechanisms by which lignin can be depolymerized is important for its removal or coutilization with carbohydrates.[12]

Lignin is comprised of three phenyl-propanoid monomers: 4-hydroxycinnamyl alcohol (H), coniferyl alcohol (G), and sinapyl alcohol (S), which are linked via C−O and C−C bonds formed by radical coupling reactions during cell wall biosynthesis.[13,14] These reactions create branched, high molecular weight polymers that plants use for defense and water transport. The predominant linkage in lignin is the aryl-ether β-O-4 bond, which often comprises up to 50% of the intermonomer linkages in most plants.[13] Lignin polymers are often terminated by a *p*-hydroxyl group (Figure 1), which is

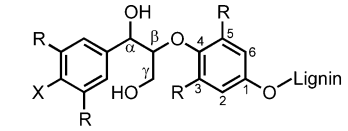

Figure 1. Lignin polymers can be terminated by a *p*-hydroxyl group or connected to additional lignin species, referred to as "phenolic" (X = OH) and "non-phenolic" (X = H or O-lignin) groups, respectively.

typically referred to as a "phenolic" group, whereas "non-phenolic" β-O-4 linkages internal to the lignin polymer will be connected to additional monomeric units. As the β-O-4 linkage is the most predominant in lignin, many fundamental studies have focused on understanding how this bond is cleaved in various physical and chemical environments or in the presence of homogeneous and heterogeneous catalysts.[15−32] Moreover, sophisticated NMR methods have been developed to fingerprint the presence of these aryl-ether linkages (and other linkages) in lignin to understand their fate as a function of treatment.[33−38]

Biomass utilization efforts for both fuels and products from carbohydrates often focus on lignin removal from, or redistribution within, biomass.[39,40] This is a technical challenge that, for example, has received significant attention in the pulping industry, wherein acid or base catalysts are used to depolymerize lignin (and often some hemicellulose) to produce pulp fibers. From the standpoint of fuels production from biomass-derived carbohydrates, thermo-chemical pretreatment strategies such as dilute acid hydrolysis, hot water pretreatment, ammonia-fiber expansion, lime, and steam explosion technologies have been developed to partially or completely remove hemicellulose, redistribute lignin, and to generally make the plant cell wall more accessible to digestion by cellulolytic enzymes.[1,10,41] Concentrated acid hydrolysis can also be applied to depolymerize hemicellulose, cellulose, and lignin. With the aim to improve carbohydrate yields from biomass, substantial efforts have also been expended to genetically modify plants to exhibit lower lignin contents or less recalcitrant lignin.[42−51] Other technologies are under development to fractionate the plant cell wall into its constituent polymers with organic solvents (Organosolv processes)[33,52,53] or novel solvents such as ionic liquids.[54−56] Organosolv processes typically utilize acid as well to depolymerize some of the lignin and hemicellulose.

A common theme in many of the biomass treatments described above is the use of acid catalysts to depolymerize and dehydrate carbohydrates. Mineral acids, for example, have been widely used for nearly a century to hydrolyze bonds in cellulose and hemicellulose, which can produce sugars or furans depending on the severity of the process conditions. Acid treatment of biomass is thought to cleave a fraction of the predominant aryl-ether linkages in lignin, the extent depending on the severity of acid treatment, as observed in NMR studies.[34,35,57,58] However, despite widespread acceptance that acid catalyzes hydrolysis of aryl-ether bonds, the mechanism by which acid cleaves β-O-4 linkages is not fully elucidated.[12] Moreover, there exist significant discrepancies between rates of cleavage of aryl-ether bonds in model compounds and in biomass-derived lignin.

Among the studies of β-O-4 cleavage, Lundquist et al. published an extensive series of elegant studies on model compounds and biomass-derived lignins, starting in the 1970s to examine acid cleavage of aryl-ether bonds.[19,59−67] Yasuda et al. also published a seminal series of studies focusing on the chemical structures of lignin (both native and models) degraded by H_2SO_4.[68−80] These two bodies of work used chromatographic methods to examine multiple questions related to lignin acidolysis mechanisms and resulted in several proposed mechanisms for β-O-4 cleavage for both non-phenolic and phenolic aryl-ether linkages. In particular, ionic mechanisms were proposed for the acid catalyzed cleavage of non-phenolic lignin model dimers through an enol-ether intermediate.[67] For phenolic lignin model dimers exhibiting the β-O-4 linkage, Lundquist et al.[19,61,81] as well as several other groups[82−86] proposed homolytic mechanisms in dioxane/water mixtures and in mild/dilute acid solutions that proceed via quinone methide intermediates. However, direct evidence of homolytic cleavage has to our knowledge not been shown for either non-phenolic or phenolic β-O-4 model systems. Density functional theory (DFT) studies have reported that the homolytic bond dissociation enthalpies of several β-O-4 models are greater than 60.0 kcal/mol, suggesting that homolytic bond cleavage will not readily occur at these temperatures.[87−89]

More recently, Matsumoto et al. investigated acid-catalyzed cleavage of aryl-ether bonds in a series of studies focused on two non-phenolic β-O-4 dimers using a range of acids including HBr, HCl, and H_2SO_4 in water−dioxane mixtures.[17,18,59,90,91] Importantly, they isolated an enol-ether intermediate 1-(2-methoxyphenoxy)-2-(3,4-dimethoxyphenyl)ethylene, shown in Figure 2A, in the acid cleavage of a model dimer, 2-(2-

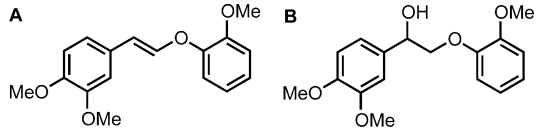

Figure 2. Enol-ether intermediate identified by Matsumoto and co-workers.[17] 1-(2-Methoxyphenoxy)-2-(3,4-dimethoxyphenyl)ethylene (A) in the acidolysis of 2-(2-methoxyphenoxy)-1-(3,4-dimethoxyphenyl)ethanol (B).

methoxyphenoxy)-1-(3,4-dimethoxyphenyl)ethanol (Figure 2B), suggesting that a primary intermediate of a proposed mechanism from Lundquist and Lundgren[67] was valid for acidolysis in HBr and dioxane/water. In all cases, they used a reaction temperature of ∼85 °C, which is lower than common temperatures for dilute acid hydrolysis of biomass, which range

dx.doi.org/10.1021/sc400384w | ACS Sustainable Chem. Eng. 2014, 2, 472−485

from ~120 °C to above 200 °C, depending on process severity.[10,41] Matsumoto et al. propose multiple reaction mechanisms primarily from identification of several intermediates.[17,18,59,90,91] Throughout these studies by Matsumoto et al., the rates of H_2SO_4 acid catalyzed β-O-4 cleavage are quite slow, often reaching only 40% conversion after 60 h.

Lastly, a number of studies have been conducted to understand the effects of acid treatment on lignin in biomass. Moxley et al. studied the structural changes in corn stover lignin during acid pretreatment using ^{31}P NMR spectroscopy.[57] They observed cleavage of aryl-ether lignin bonds at pretreatment conditions of 1.0% (v/v) H_2SO_4 at 140 °C in just 3 min, a much faster rate than reported by Matsumoto et al. on lignin model compounds. Similarly, Maciel et al. employed both *in situ* and *ex situ* NMR methods to examine the effect of sulfuric acid pretreatment on lignin in poplar.[34,35] They report disruption of aryl-ether bonds in lignin in as little as 5−10 min at 150 °C. These studies show that at least a fraction of native lignin degrades relatively quickly under acidolysis conditions. Ragauskas and co-workers have also examined multiple varieties of Organosolv pretreatment and dilute acid pretreatment with NMR methods and found similar time scales for partial aryl-ether bond cleavage.[12,58,92,93]

Here, we seek to understand the fundamental mechanisms of acid cleavage of aryl-ether linkages in lignin at conditions similar to dilute acid pretreatment (i.e., aqueous phase H_2SO_4 at 150 °C). In particular, we aim to understand from a mechanistic perspective the disparity in time scales between acidolysis of lignin model compounds and biomass-derived lignin. We examine four lignin model compounds that exhibit the β-O-4 linkage with or without a neighboring phenolic hydroxyl group, shown in Figure 3. Experimental data obtained

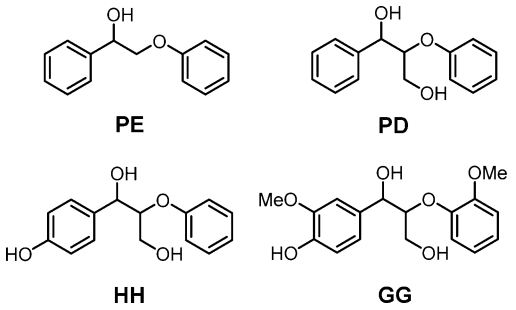

Figure 3. Model compounds used in this study. 2-Phenoxy-1-phenylethanol (**PE**), 1-phenyl-2-phenoxy-1,3-propanediol (**PD**), 1-(4-hydroxyphenyl)-2-phenoxy-1,3-propanediol (**HH**), and 1-(4-hydroxy-3-methoxyphenyl)-2-(2-methoxyphenoxy)-1,3-propanediol (**GG**).

in this work show that the presence of a phenolic hydroxyl group dramatically increases the rate of acid-catalyzed β-O-4 bond cleavage and that the presence of a methoxy group on the phenyl ring alters the product distribution. To understand the mechanisms for each model compound, we experimentally identify intermediate products and examine the structures and thermodynamics of intermediates of interest along each reaction pathway with DFT calculations.

Before presenting the results in detail, we stress that the DFT calculations do not address the specific rates (kinetics) at which products are formed, only the relative stabilities (thermodynamics) of proposed intermediates. The DFT calculations do, however, show that the proposed pathways are energetically feasible and are primarily used to interpret the reactivity differences between the phenolic and non-phenolic model dimers. Therefore, it is important not to overinterpret the potential energy surfaces relative to the experimentally observed product distributions. Moreover, we do not explicitly model the solvent (water) in the DFT calculations, and the relative thermodynamics of both the carbocation and protonated species along the reaction pathways will likely behave differently in explicit solvent. The thermodynamics of transient species in implicit solvent DFT calculations are presented primarily to complete the mechanistic steps for catalysis of these model dimers under acidic conditions.

RESULTS

Acidolysis of Non-phenolic and Phenolic Lignin Model Compounds. To determine the fate of β-O-4 ether linkages under process-relevant acid pretreatment conditions, the model compounds **PE**, **PD**, **HH**, and **GG** were subjected to acidolysis in 0.2 M H_2SO_4 at 150 °C in water. The products of acidolysis were identified by GC-MS, and the concentrations and kinetics were determined from HPLC. The acidolysis of **PE** and **PD** yields similar product distributions (Figure 4A) at similar rates (Figure 4B). Pseudo-first-order rate constants for the conversion of **PE** and **PD** are 2.2×10^{-2} h^{-1} and 2.0×10^{-2} h^{-1} respectively. These rates are similar to those reported by Matsumoto et al. for the acidolysis of non-phenolic 2-(2-methoxyphenoxy)-1-(3,4-dimethoxyphenyl)-propane-1,3-diol in H_2SO_4 (0.81×10^{-2} h^{-1}).[90] Under these acidolysis conditions, both non-phenolic models (**PE** and **PD**) yield phenol (**POH**) and phenylacetaldehyde (**PAA**), where this latter product is formed via loss of the γ-carbinol group presumably as formaldehyde from cleavage of the $\beta-\gamma$ carbon−carbon bond via a retro-Prins reaction in **PD**.[94] The loss of the γ-carbinol group as formaldehyde is well characterized in the literature by the detection of products from the condensation of formaldehyde with two aromatic units to form a diphenylmethane type structure.[71,95] However, trace amounts of minor products, 1-hydroxy-3-phenyl-2-propanone (1-phenylacetylcarbinol, **PAC**) are detected in the product distribution of **PD**, suggesting that acidolysis of **PD** proceeds via two pathways: one similar to that of **PE** and another in which the γ-carbinol is retained during β-O-4 cleavage. As discussed below, all three of the γ-carbinol containing model compounds (**PD**, **HH**, and **GG**) show evidence of acidolysis conversion through divergent pathways in the form of similar γ-carbinol containing intermediates as well as phenylacetylcarbinol products. The divergent pathways were observed in Lundquist's early studies[62−67] as well as subsequent studies on lignin model compounds.[18,59,90,91,95] There is also a small amount of a self-condensation product, 3-phenyl-2,3-dihydrobenzofuran-2-ol (**PBF**), which is quite stable. The guaiacyl type of this self-condensation product has been observed in other lignin model compound studies by Yasuda et al.[70]

The phenolic model compounds, **HH** and **GG**, also produce an aldehyde and either **POH** or guaiacol (**GOH**), respectively under acidolysis conditions, as well as other products (Figure 4A). However, the rate of loss of **HH** and **GG** is dramatically increased relative to that of **PE** and **PD** (Figure 4B), with pseudo-first-order rate constants of 1.1 and 1.5 h^{-1}, respectively. Major products of **HH** acidolysis include **POH** and (4-hydroxyphenyl)-acetaldehyde (**HPA**). There exists evidence of the aforementioned second pathway, as trace amounts of 1-hydroxy-3-(4-hydroxyphenyl)-2-propanone

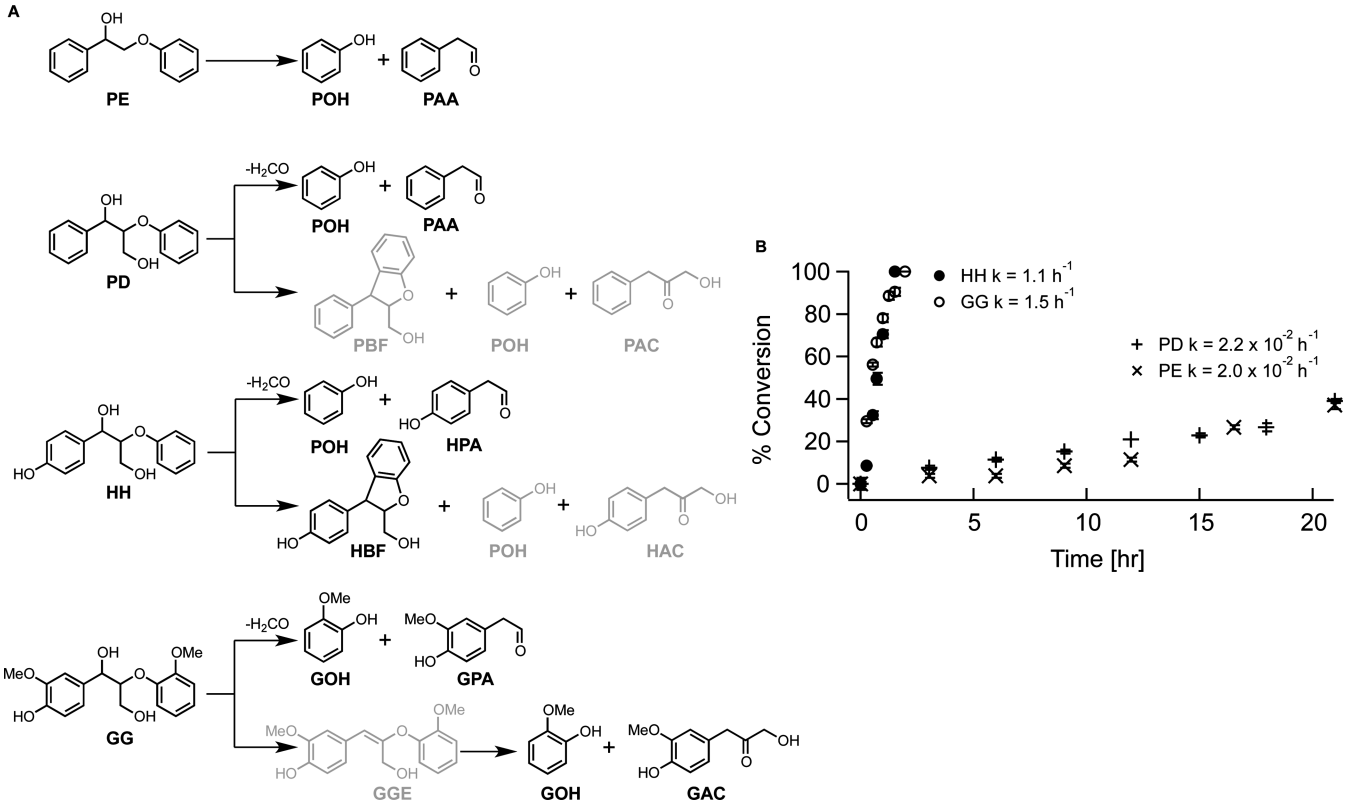

Figure 4. (A) Product distribution upon acidolysis (0.2 M H_2SO_4, 150 °C) with minor products shown in gray. (B) Conversion of PE, PD, HH, and GG over time; k = pseudo-first-order rate constants for loss of each model compound.

(**HAC**) are detected. Self-condensation of **HH** via a carbocation intermediate produces 3-(4-hydroxyphenyl)-2,3-dihydrobenzofuran-2-ol (**HBF**). This byproduct was also found to be quite stable. Acidolysis of **GG** yields G-type analogues of **HH** products: guaiacol (**GOH**), (4-hydroxy-3-methoxyphenyl) acetaldehyde (**GPA**), and 1-hydroxy-3-(4-hydroxy-3-methoxyphenyl)propan-2-one (**GAC**). The presence of **GAC** as a major product and detection of the enol ether intermediate, 3-(4-hydroxy-3-methoxyphenyl)-2-(2-methoxyphenoxy)-2-propenol (**GGE**), during the reaction suggests that **GG** conversion proceeds through both divergent pathways at equal rates. The presence of the methoxy groups on the phenyl rings of **GG** prevents formation of a phenyldihydrobenzofuran byproduct thereby allowing conversion to proceed through the second pathway.

The disparity in β-O-4 cleavage time scales between non-phenolic **PE**/**PD** and phenolic **HH**/**GG** under these conditions shows that the presence of a phenoxy hydroxyl group greatly enhances the rate of β-O-4 cleavage. Below, we present a detailed experimental and theoretical analysis of each reaction pathway to understand the observed disparities in time scales and product distributions, with the aim to use these model systems to interpret observations related to the mechanism of lignin acidolysis in biomass pretreatment, fractionation, or acid-based pulping.

Acid-Catalyzed Conversion of PE. First, we examined the acidolysis of **PE**, a simple non-phenolic β-O-4 model dimer that does not exhibit a γ-carbinol group. Figure 5 shows the concentration of **PE**, **POH**, and **PAA** during acidolysis as a function of time. The conversion of **PE** is relatively slow, reaching only 40% in 21 h. **PE** conversion produces few if any byproducts (based on GC-MS and HPLC analysis) with a yield

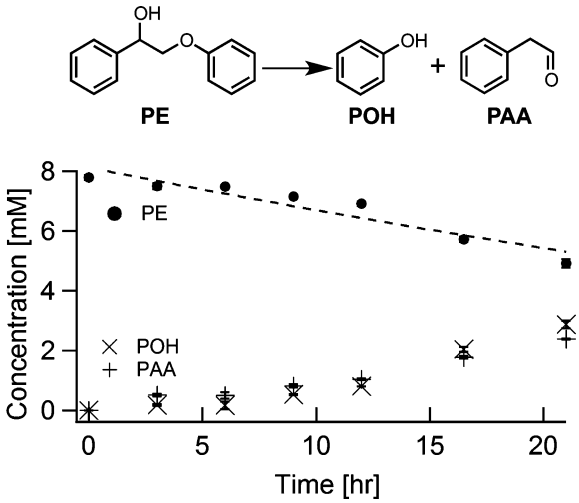

Figure 5. PE acidolysis: conversion reaction and change in concentrations of **PE**, **POH**, and **PAA**.

of 99% based on recovered starting materials (BRSM). Two mechanisms were proposed for β-O-4 cleavage of **PE** to yield **POH** and **PAA**. In the first proposed mechanism (**PE**-mechanism 1, Figure 6), **PE** is protonated at the α-hydroxyl group (**PE-1**) followed by dehydration to form a carbocation (**PE-2**). Abstracting a proton from **PE-2** produces an enol-ether intermediate (**PE-3**). Protonation of **PE-3** produces a resonance-stabilized intermediate (**PE-4**). The β-carbon is hydrated followed by deprotonation (**PE-5** and **PE-6**, respectively). **PE-6** is then cleaved to form the products, **POH** and **PAA**. After the initial dehydration forming the

dx.doi.org/10.1021/sc400384w | ACS Sustainable Chem. Eng. 2014, 2, 472−485

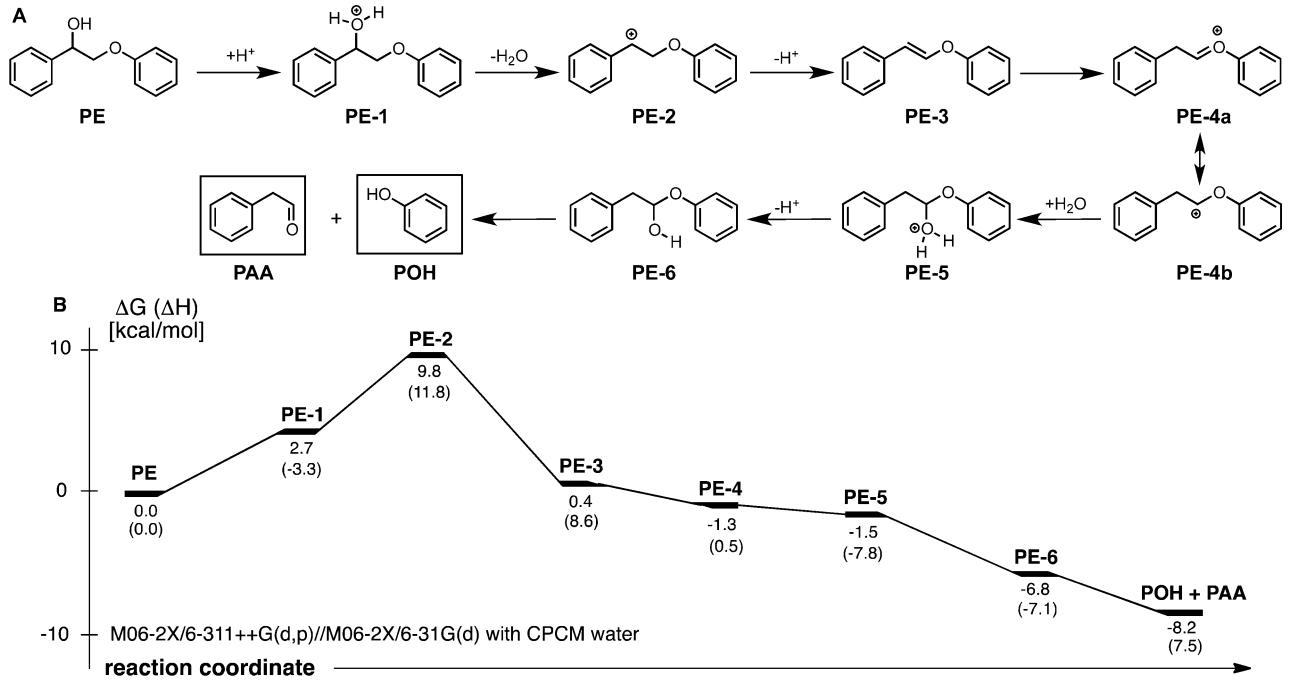

Figure 6. **PE**-mechanism 1 (A) and reaction energy diagram (B) for **PE** conversion to **POH** and **PAA** through an enol-ether intermediate (**PE-3**).

carbocation (**PE-2**), formation of the products is exergonic (ΔG = −8.2 kcal/mol overall reaction pathway).

In a second proposed mechanism (**PE**-mechanism 2, Figure S1), the ether oxygen is directly protonated and the β-O-4 bond is cleaved resulting in an epoxide and **POH**. This epoxide can then take several routes to the product **PAA**, including a pinacol rearrangement. Alternatively, the epoxide can be hydrated and subsequently deprotonated to form a diol, which can then be protonated and dehydrated to form a species that will tautomerize to the product **PAA**.

The initial steps of **PE**-mechanism 1, **PE** to **PE-2** (ΔG = 9.8 kcal/mol), are more thermodynamically favorable than those proposed in **PE**-mechanism 2. These hypothesized mechanisms led us to analyze trace compounds using GC-MS to determine which pathway was more likely, based on the presence of proposed intermediates. Indeed, trace amounts of **PE-3** were detected in GC-MS analysis, but **PE-3** concentrations did not accumulate sufficiently to quantify the amount present at any time, in turn suggesting that conversion of **PE-3** to **POH** and **PAA** is rapid at these conditions. To confirm that **PE-3** is an intermediate and that **PE** acidolysis proceeds via **PE**-mechanism 1, **PE-3** was synthesized and under acidolysis conditions was shown to convert to **POH** and **PAA** (Figure S2). This conversion is extremely fast relative to **PE** conversion and reached 70% conversion in 1 h. There was no experimental evidence of the epoxide or diol, the proposed intermediates of **PE**-mechanism 2, at any time. In light of these results, **PE**-mechanism 1 is the most likely pathway for **PE** conversion. Direct protonation at the ether oxygen was therefore not considered in the conversion mechanisms of the other model compounds.

Acid-Catalyzed Conversion of PD. **PD** is the second non-phenolic β-O-4 dimer considered here, which exhibits the γ-carbinol group found in native lignin. Figure 7 shows the product distribution of **PD** acidolysis and the concentrations of reactants and detected products as a function of time. Although the addition of the γ-carbinol group does not affect the rate of

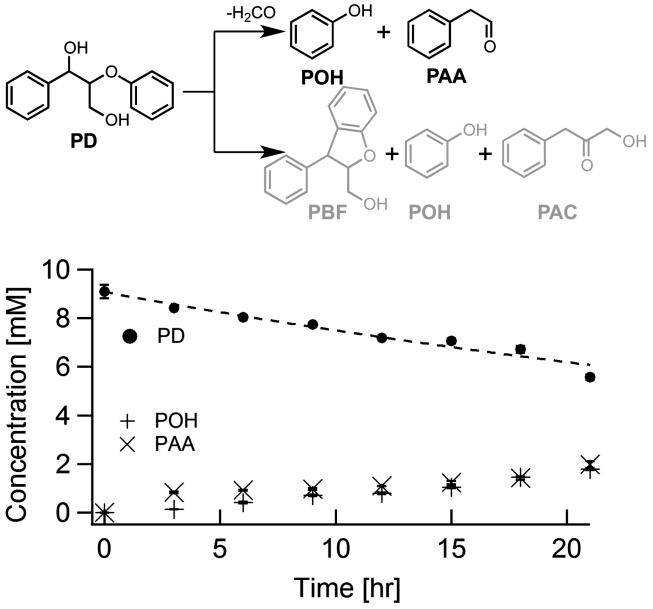

Figure 7. **PD** acidolysis: conversion reaction and change in concentrations of **PD**, **POH**, and **PAA**. Minor products were not quantified.

acidolysis, the conversion of **PD** yields a slightly different product distribution than **PE**: **POH** and **PAA**, with trace amounts of **PAC** and **PBF**.

The measured product yield was low (56% BRSM), indicating that additional products were formed (e.g., **PAC** and **PBF** were detected). In addition to the detected products, evidence of charring is evident in the discoloration of samples after 12 h. The major product distribution from the conversion of **PD** indicates that the γ-carbinol group is lost during acidolysis. This same phenomenon has previously been studied and attributed to β−γ carbon−carbon bond cleavage accompanied by the loss of formaldehyde.[71,95] Matsumoto et

dx.doi.org/10.1021/sc400384w | ACS Sustainable Chem. Eng. 2014, 2, 472−485

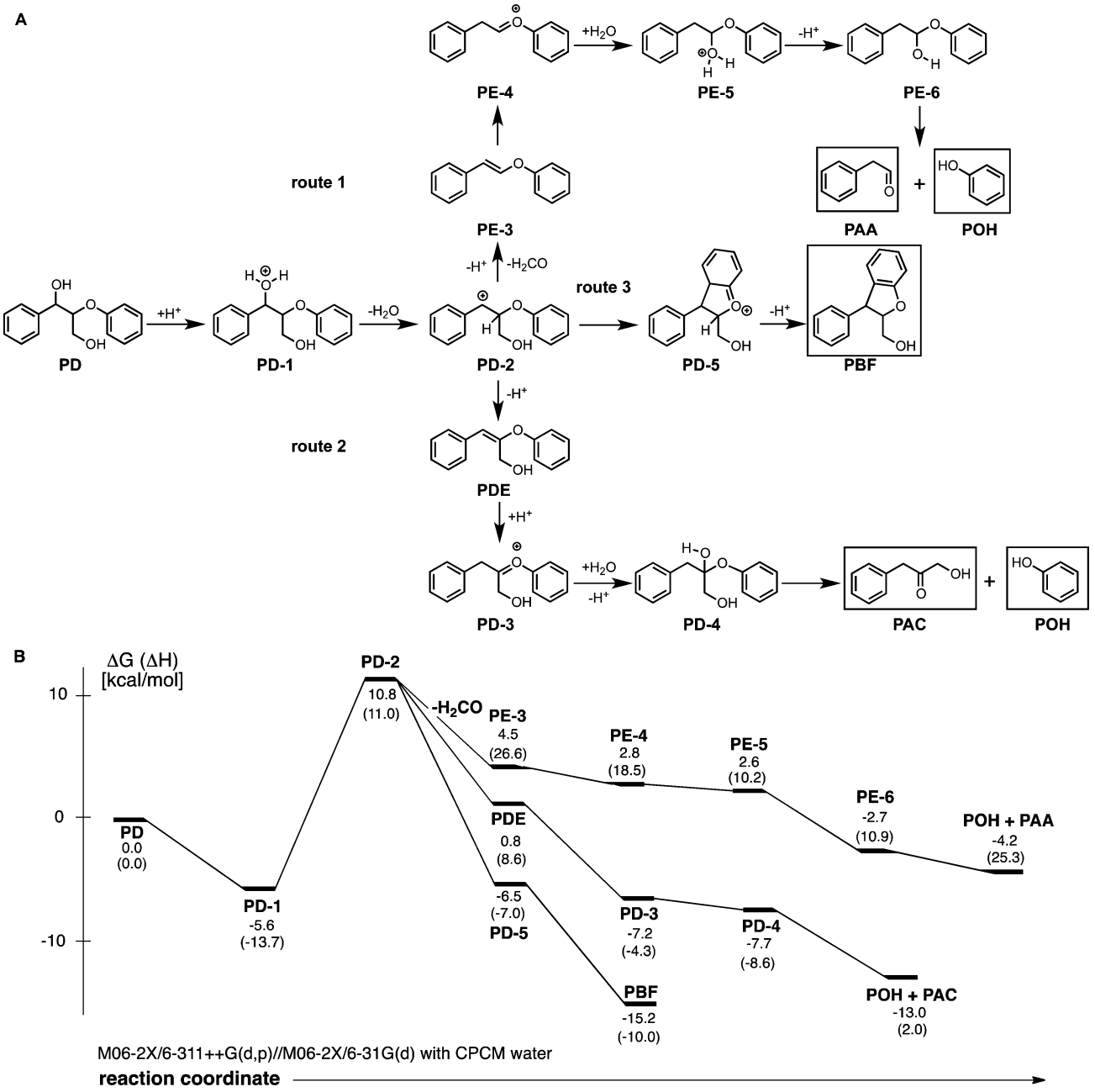

Figure 8. Proposed **PD**-mechanism 1, routes 1, 2, and 3 (A) and reaction energy diagram (B) for **PD** conversion.

al. observe similar products in the acidolysis of lignin model compounds with H_2SO_4 and speculate that the γ-carbinol group is lost as undetected formaldehyde.[90] We were unable to detect formaldehyde in any form in our experiments and speculate that some of the solids formed and charring observed were due to polymerized formaldehyde.

In addition to the major products (**POH** and **PAA**), trace amounts of **PAC** and **PBF** were detected in GC-MS analysis. These γ-carbinol containing species suggest **PD** conversion proceeds through one mechanism with three possible routes. Potential conversion routes of **PD** to major products (**POH** and **PAA**), minor products (**POH** and **PAC**), and the **PBF** byproduct with associated energy diagrams are proposed in Figure 8.

In the first route for **PD** conversion (**PD**-route 1, in Figure 8), the α-hydroxyl group is protonated (**PD-1**) followed by dehydration to form a carbocation (**PD-2**). This is the least thermodynamically favorable step of **PD**-route 1 (ΔG = 16.2 kcal/mol). In the following step, the γ-carbinol from **PD-2** is released as formaldehyde, resulting in the formation of an enol-ether intermediate (**PE-3**), which is identical to the intermediate from **PE** conversion (**PE**-mechanism 1). As such, the following steps are identical to those shown in the **PE**-mechanism 1 of **PE** conversion and result in **POH** and **PAA** as final products via β-O-4 bond cleavage.

In the second proposed route for **PD** conversion (**PD**-route 2, in Figure 8), the initial steps to **PD-2** are identical to those proposed in **PD**-route 1; however, in the subsequent steps the γ-carbinol moiety is retained and conversion proceeds through **PDE** to form **POH** and **PAC**. According to **PD**-route 2, **PD-2** is deprotonated at the β- position forming a C_α=C_β double bond (**PDE**). **PDE** is protonated, and the positive charge is

dx.doi.org/10.1021/sc400384w | ACS Sustainable Chem. Eng. 2014, 2, 472−485

resonance-stabilized (**PD-3**). The β-carbon is then hydrated followed by deprotonation (**PD-4**). The β-O-4 ether bond in **PD-4** is cleaved to yield the products, **POH** and **PAC**. The dehydration step leading to **PD-2** is the least thermodynamically favorable, but the subsequent steps are mainly exergonic. Alternately, the benzyl carbocation intermediate **PD-2** could undergo self-condensation via electrophilic aromatic substitution to form the observed byproduct **PBF** (**PD**-route 3 in Figure 8).

Experimental evidence based on the concentration of the observed major products suggests that **PD**-mechanism 1, route 1 (through intermediate **PE-3**) is favored over **PD**-route 2 and **PD**-route 3. If **PD** conversion proceeds via **PD**-route 1 and **PD**-route 2 at similar rates, the product distribution of **POH, PAA**, and **PAC** should be 2:1:1. As **POH** and **PAA** concentrations are similar, with only trace amounts of **PAC** detected, it is proposed that **PD**-route 1 is the major pathway for **PD** conversion, with minor conversion through **PD**-route 2. As the overall **PD** conversion was low (~40% at 21 h), only small amounts of **PBF** were formed through **PD**-route 3, insufficient amounts to analyze quantitatively. Further insights into this self-condensation byproduct pathway were gained in the study of **HH** acidolysis.

Acid-Catalyzed Conversion of HH. Acidolysis of **HH**, the phenolic analogue of **PD**, yields a similar product distribution to that of **PD**. However, the addition of the phenolic hydroxyl group enhances the conversion rate by 2 orders of magnitude, thereby increasing conversion from 40% at 21 h to 100% in 90 min. In addition to the two major products similar to those seen in **PD** acidolysis (**POH** and the phenolic aldehyde **HPA**), a third major product, **HBF**, is observed (Figure 9). Trace amounts of **HHE** and **HAC** are detected in the product distribution as well. Charring is also visually observed at acidolysis times greater than 45 min.

As with **PD**, we propose that **HH** acidolysis proceeds through one mechanism with three possible pathways: **HH**-mechanism 1, routes 1, 2, and 3. Proposed **HH**-routes 1−3 along with the corresponding free energy diagram are shown in Figure 10. In the first pathway, the γ-carbinol group is lost, leading to **POH** and **HPA** (**HH**-route 1 in Figure 10). In the second proposed pathway (**HH**-route 2), the γ-carbinol group is retained and conversion proceeds through **HHE** to **POH** and **HAC**. **HBF** is formed by electrophilic aromatic substitution of the phenyl ring on the carbocation intermediate **HH-2** (**HH**-route 3), as proposed in **PD** conversion (**PD**-route 3). The phenyl ring attacks the carbocation first through **HH-9** and deprotonates to form **HBF**.

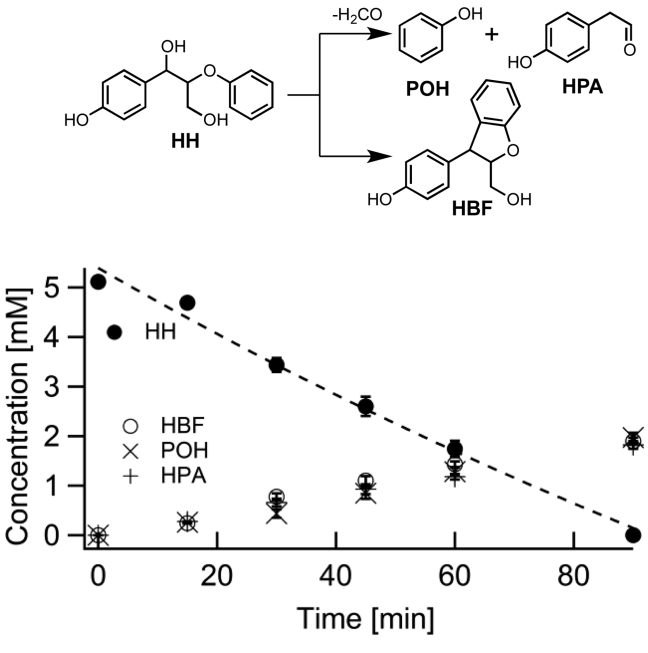

Figure 9. **HH** acidolysis: conversion reaction and change in concentrations of **HH**, **HBF**, **POH**, and **HPA**.

In **HH**-route 1, the α-hydroxyl group is protonated (**HH-1**) and dehydrates to form a carbocation intermediate (**HH-2**). The energy change for this process (**HH-1** to **HH-2**) is only ΔG = 5.3 kcal/mol compared to 16.2 kcal/mol for the corresponding process (**PD-1** to **PD-2**) in **PD** because the phenolic hydroxyl group is involved in resonance stabilization of the carbocation (**HH-2**). The enol-ether type intermediate (**HH-3**) is formed after releasing formaldehyde from the β-position and deprotonating the α-position. This step is thermodynamically unfavorable (ΔG = 13.4 kcal/mol) as a result of the resonance stabilization in **HH-2**. Deprotonation of **HH-3** forms a resonance-stabilized intermediate (**HH-4**), which is hydrated at the β-carbon (**HH-5**) and deprotonated (**HH-6**). **HH-6** gives rise to **POH** and **HPA** after hydrolysis of the β-O-4 bond. DFT calculations show that the overall reaction is slightly exergonic (ΔG = −3.1 kcal/mol) with a large change (ΔG = 13.4 kcal/mol) in free energy during the release of formaldehyde (**HH-2** to **HH-3**).

The first steps of **HH**-route 2 are identical to those in **HH**-route 1, owing to the formation of a resonance-stabilized carbocation intermediate (**HH-2**). However, in the subsequent steps of **HH**-route 2, the γ-carbinol moiety is retained and conversion proceeds through **HHE** to **POH** and **HAC**. Deprotonation of **HH-2** at the α-carbon yields **HHE**. Subsequent deprotonation at the β-position forms the resonance-stabilized **HH-7** intermediate. Hydration of **HH-7** at the β-position followed by deprotonation yields **HH-8**. The β-O-4 ether bond in **HH-8** is cleaved to release **POH** and **HAC**. Only trace amounts of **HHE** and **HAC** are observed experimentally. This is attributed to the formation of **HBF** (through **HH**-route 3) which terminates **HH**-route 2 by converting available **HH-2** to **HBF**.

Analysis of the product distribution shows that **POH**, **HPA**, and **HBF** are all formed at similar rates (Figure 9) and the final product concentrations and yields (based on **HH** conversion) of **POH** (1.97 mM, 39%), **HPA** (1.82 mM, 36%), and **HBF** (1.90 mM, 37%) are similar. As only trace amounts of **HHE** and **HAC** are experimentally observed, thus it is assumed that formation of **HBF** terminates **HH**-route 2. The total product recovery yield was 76% BRSM, with some loss of product due to visibly noticeable charring.

Lastly, an alternative mechanism has been proposed for phenolic β-O-4 dimer cleavage, namely a radical pathway.[19,61,81−86] To test the possibility of **HH** degradation through a homolytic cleavage pathway under these acidolysis conditions, a radical scavenger, butylated hydroxytoluene (BHT), was added to a reaction mixture containing **HH** and 0.2 M H_2SO_4 and subjected to acidolysis conditions. The **HH** sample containing the BHT exhibits an identical rate of disappearance to **HH** with no BHT (Figure S3). No evidence of homolytic cleavage was observed, as the product distribution was identical to that seen in **HH** acidolysis. These results

dx.doi.org/10.1021/sc400384w | ACS Sustainable Chem. Eng. 2014, 2, 472−485

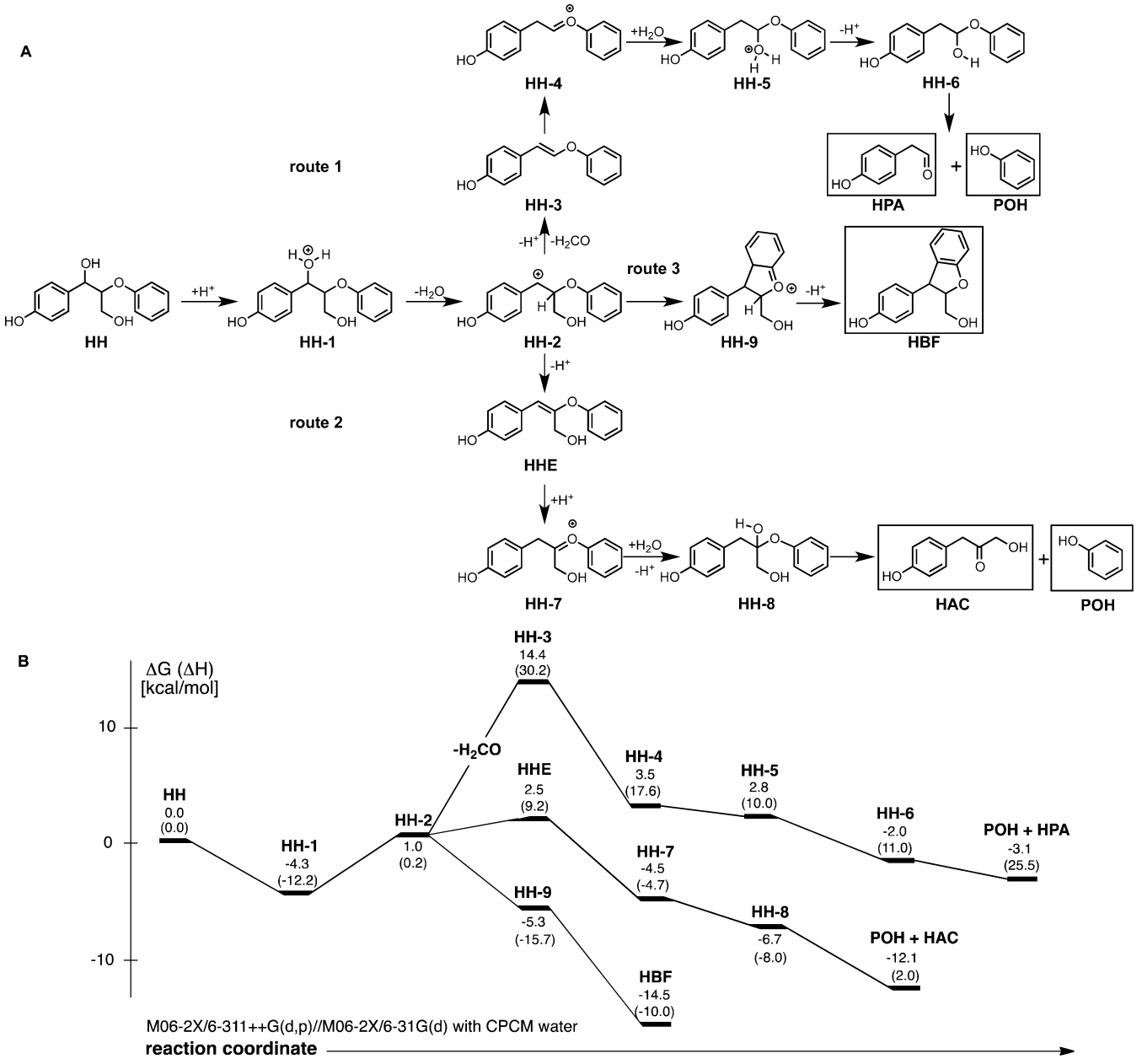

Figure 10. Proposed **HH**-mechanism 1, routes 1, 2, and 3 (A) and reaction energy diagram (B) for **HH** conversion.

suggest homolytic cleavage of phenolic lignin model compounds is unlikely at 150 °C under these acidic conditions.

Acid-Catalyzed Conversion of GG. **GG** is a phenolic lignin model compound with a methoxy substituent on each of the phenyl rings. Under the acidolysis conditions employed here, **GG** rapidly converts to **GOH**, **GPA**, and **GAC** (Figure 11). Similar to **HH**, the rate of conversion of **GG** is nearly 2 orders of magnitude faster than **PE** and **PD** conversion.

Similar to **PD** and **HH**, the acidolysis of **GG** is proposed to proceed through one mechanism with two routes (Figure 12). The intermediate **GGE** is observed in the first 20 min of acidolysis and is quickly consumed via **GG**-route 2. The presence of a methoxy moiety on the phenyl rings of **GG** prevents the formation of the phenyl-dihydrobenzofuran species (**PBF** and **HBF** in **PD**-route 3 (Figure 8) and **HH**-route 3 (Figure 10), respectively), as no such species was detected experimentally in the acidolysis of **GG**. The proposed mechanism with **GG**-route 1, loss of the γ-carbinol group yielding **GOH** and **GPA**, and **GG**-route 2, proceeding through γ-carbinol containing intermediate **GGE** yielding **GOH** and **GAC**, are presented in Figure 12 along with their associated free energy diagrams.

As **GG** is the methoxy-containing analogue of **HH**, proposed acidolysis conversion **GG**-route 1 and **GG**-route 2 proceed in an analogous manner as **HH** conversion, albeit with methoxy-modified intermediates and products and slightly different energetics. In **GG**-route 1, the α-hydroxyl group is protonated and dehydrated to form a carbocation intermediate (**GG-2**). The energy difference for this process (**GG-1** to **GG-2**) is ΔG = 10.1 kcal/mol compared to 5.3 kcal/mol for the corresponding process with **HH** (**HH-1** to **HH-2**) indicating that the presence of a methoxy group disrupts the resonance-stabilized carbocation (**GG-2**). Loss of formaldehyde from the β-position, accompanied with deprotonation at the α-position,

dx.doi.org/10.1021/sc400384w | ACS Sustainable Chem. Eng. 2014, 2, 472−485

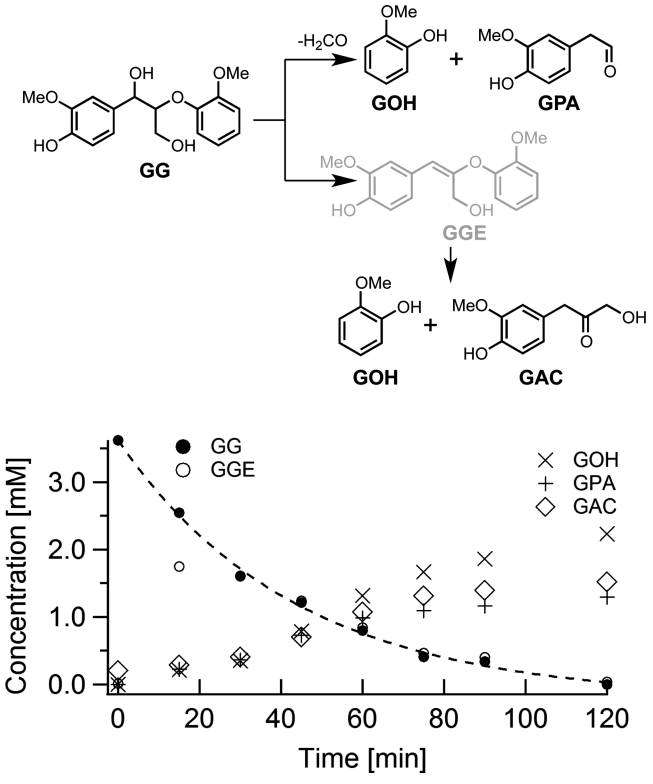

Figure 11. **GG** acidolysis: conversion reaction and change in concentrations of **GG**, **GGE**, **GOH**, **GPA**, and **GAC**.

yields the enol-ether intermediate (**GG-3**) (ΔG = 14.6 kcal/mol). Deprotonation of **GG-3** forms a resonance-stabilized intermediate (**GG-4**), which is hydrated at the β-carbon (**GG-5**) and deprotonated (**GG-6**). After acid hydrolysis of the β-O-4 bond, **GG-6** yields **GOH** and **GPA**. DFT calculations show that the overall reaction is exergonic (ΔG = −7.9 kcal/mol), with a large change in free energy upon formaldehyde release.

In **GG**-route 2, the γ-carbinol moiety is retained and **GG** conversion proceeds through **GGE** to **GOH** and **GAC**. **GG-2** is deprotonated at the α-carbon producing **GGE**. Subsequent deprotonation forms **GG-7** which is hydrated at the β-position followed by deprotonation to give **GG-8**. The β-O-4 ether bond in **GG-8** is cleaved to release **GOH** and **GAC**. The overall computed ΔG value for **GG**-route 2 is −17.2 kcal/mol. The difference in calculated ΔG values between **GG**-routes 1 and 2 is −9.3 kcal/mol.

Unlike **PD** and **HH**, where **GG**-route 2 is terminated by formation of the phenyl-dihydrobenzofuran species (**PBF** and **HBF**) from **PD**-2 and **HH**-2, a **G** type phenyl-dihydrobenzofuran species is not formed during **GG** conversion. The presence of the *ortho*-electron withdrawing methoxy group hinders the formation of the phenyl-dihydrobenzofuran species by blocking an *ortho* position, as well as deactivating the ring, making the aromatic group less prone to undergo electrophilic aromatic substitution, thereby allowing **GG-2** to proceed via **GG**-route 2, through **GGE**, to form **GOH** and **GAC**. The final product distribution from **GG** conversion is expected to proceed through the two pathways at similar rates: **GOH** = 2.23 mM, 64%; **GPA** = 1.30 mM, 36%; and **GAC** = 1.52 mM, 42%. The total recovered product yield was 64% BRSM again showing some loss of product due to charring.

DISCUSSION

In the acidolysis of the four model compounds studied, only the γ-carbinol containing **PD, HH**, and **GG** show evidence of simultaneous conversion through multiple routes. Cleavage of these model compounds proceeds through both loss of the γ-carbinol group and through formation of phenyl-dihydrobenzofuran in the acidolysis of both **PD** and **HH** (routes 1 and 3 in Figures 8 and 10) or via formation of **GOH** and **GAC** in the acidolysis of **GG** (routes 1 and 2 in Figure 12). Loss of the γ-carbinol group during acidolysis of model compounds **PD**, **HH**, and **GG** (route 1) is an irreversible process proceeding to the formation of phenol (**PD** and **HH**) or guaiacol (**GG**) and **PAA**, **HPA**, or **GPA** (**PD**, **HH**, and **GG**, respectively). As the products resulting from β-O-4 cleavage via route 2 or 3 are more thermodynamically stable than those resulting from route 1 (ΔG: **PD**-route 1: **POH** + **PAA** = −4.2 kcal/mol; **PD**-route 2: **POH** + **PAC** = −13 kcal/mol; **PD**-route 3: **PBF** = −15.2 kcal/mol; **HH**-route 1: **POH** + **HPA** = −3.1 kcal/mol; **HH**-route 2: **POH** + **HAC** = −12.1 kcal/mol; **HH**-route 3: **HBF** = −14.5 kcal/mol; **GG**-route 1: **GOH** + **GPA** = −7.9 kcal/mol; **GG**-route 2: **GOH** + **GAC** = −17.2 kcal/mol), the loss of the γ-carbinol moiety must therefore be kinetically driven. The experimentally observed product distributions in both **HH** and **GG** acidolysis suggest that flux through route 1 is equal to route 3 (**HH**) or route 2 (**GG**), as the ratio of products from each are 1 to 1 (route 1 to route 3 (**HH**) and route 1 to route 2 (**GG**)). Recovered product yields of these compounds were low: 56% (**PD**), 76% (**HH**), and 64% (**GG**). Visually observed charring is responsible for these lowered yields. Condensation of deconstructed lignin byproducts is well-known[34] and also thought to contribute to lower yields.

The presence of the phenolic hydroxyl group in **HH** and **GG** increased the rate of β-O-4 bond cleavage by 2 orders of magnitude over the non-phenolic models, **PE** and **PD**. This increase in rate is thought to be due to stabilization of the carbocation intermediate **HH-2** and **GG-2** via delocalization of benzylic carbocation. This increase in rate was not previously observed in studies from Matsumoto et al., as their model compounds were all non-phenolic.[17,18,59,90,91]

The benzylic carbocationic intermediates **PD-2** and **HH-2** are formed via protonation of the α-hydroxyl group followed by dehydration. DFT results show the relative free energies of these intermediates are 10.8 and 1.0 kcal/mol above their respective starting compounds (Figure 13). The relative stabilization of **HH-2** relative to **PD-2** arises due to delocalization of the benzylic carbocation onto the *para*-hydroxyl group, which may be rationalized in terms of canonical resonance structures, and is also evident from the computed charges shown in Figure 13. Distortion of the aromatic ring in cation **HH-2** toward a formal quinone methide Lewis structure is readily apparent in Figure 13, and atomic charges following a natural population analysis (NPA) also show the charge at the benzylic carbon is reduced by the para-OH substituent (from 0.10 to 0.03).

In contrast with unsubstituted substrate **PD**, for which carbocation formation acts as the energetic bottleneck toward conversion, the relative stabilization of carbocationic intermediate **HH-2** provides a much more energetically favorable pathway for **HH** to convert toward products. We reason based on the Hammond postulate that these lower computed free energy changes will be accompanied by lower barrier heights, which will thus mean that **HH** reacts much more quickly, which

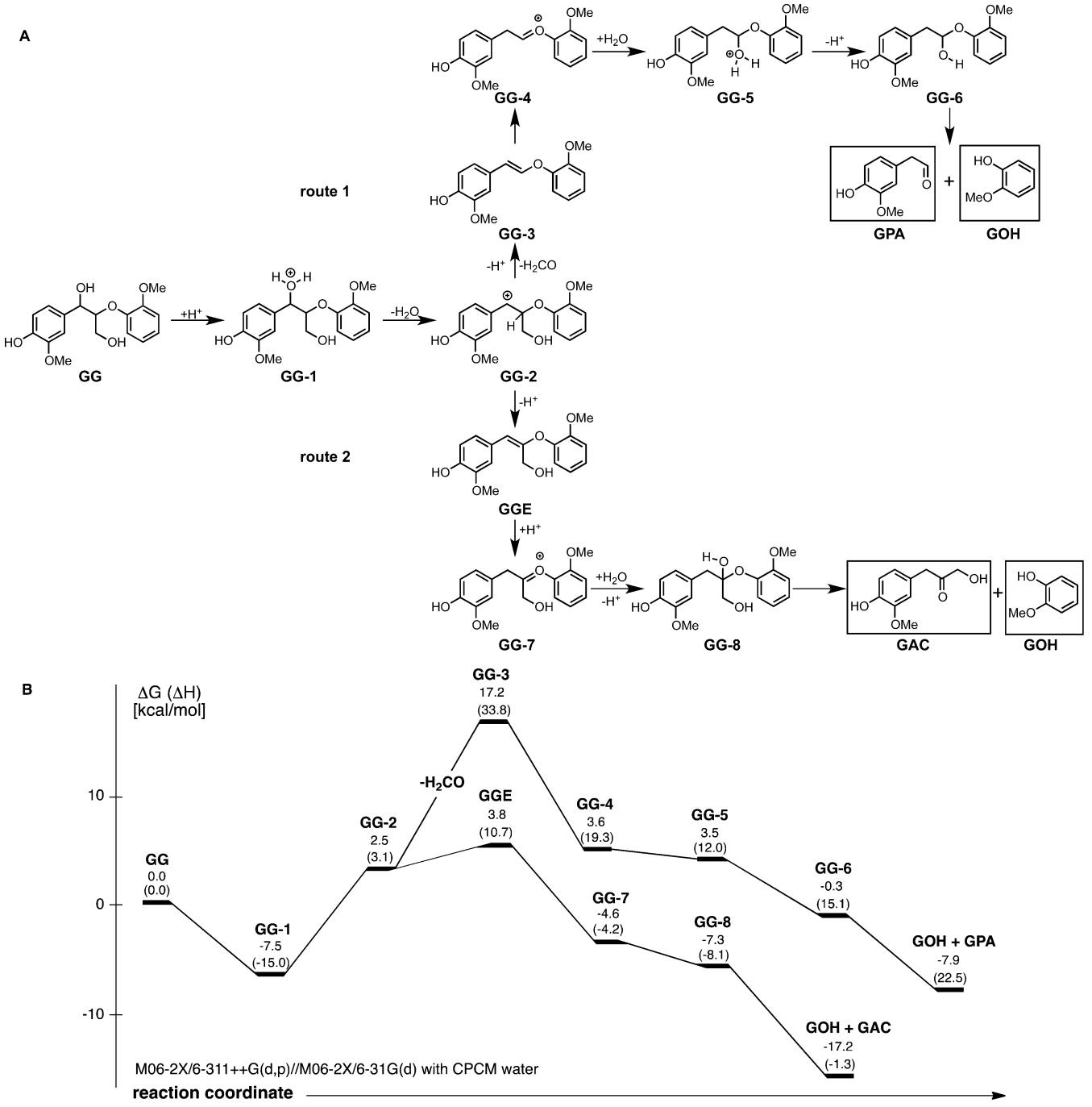

Figure 12. Proposed **GG**-mechanism 1, routes 1 and 2 (A) and reaction energy diagram (B) for **GG** conversion.

is observed experimentally. Similar stabilization occurs in **GG**, accounting for the increased rate of conversion compared to non-phenolic **PD**.

Formation of the phenyl-dihydrobenzofuran species upon acidolysis was not observed in past studies by Lundquist et al.,[19,59−67] Yasuda et al.,[68−80] and Matsumoto et al.[17,18,59,90,91] as their model compounds all contained *ortho* methoxy substituents on the aryl rings (modeling **G** and **S** type lignins). As previously stated, the presence of the *ortho* methoxy group deactivates the ring and blocks a reaction site, thus preventing the formation of a phenyl-dihydrobenzofuran type byproduct and allowing for **GG** acidolysis to proceed via **GG**-route 2, consistent with experimantal observations. DFT results also suggest the relative free energies of **HH-2** and **GG-2** are 1.0 and 2.5 kcal/mol above their respective starting compounds. The relative destabilization of **GG-2** compared to **HH-2** is due to the methoxy substituent. The methoxy group *ortho* to the hydroxyl group is electron-withdrawing, which diminishes the resonance stabilization, directing acid hydrolysis to proceed through **GG**-route 2.

Taken together, the rates of *β*-O-4 cleavage in **HH** and **GG** would seem to indicate that the relatively fast rate of *β*-O-4 cleavage observed in native lignin[12,34,35,57,58,92,93] could be due to terminal hydroxyl groups and depolymerization proceeding via an unzipping mechanism. In the acidolysis of native lignins containing *ortho* methoxy groups (**G** and **S** type lignins) one would not expect to see self-condensation resulting in formation of a phenyl-dihydrobenzofuran. However, in **H**

dx.doi.org/10.1021/sc400384w | ACS Sustainable Chem. Eng. 2014, 2, 472−485

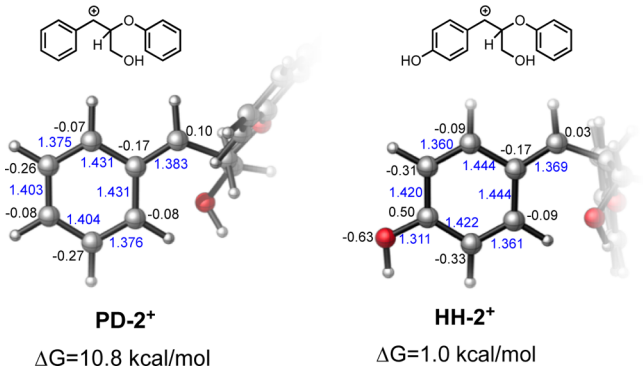

Figure 13. M06-2X/6-311++G(d,p)//M06-2X/6-31G(d) relative free energies, bond distances (Å), and NPA atomic charges for carbocation intermediates illustrate the stabilizing effect of the *para*-hydroxy substitution.

type lignin (no substituents on the phenyl rings), one would expect a significant amount of a phenyl-dihydrobenzofuran type byproduct to be formed upon acid treatment.

CONCLUSIONS

In this study, we examined four model lignin dimers of increasing complexity and substitution patterns with the aim to understand the relative reactivity and chemical pathways that β-O-4 bond cleavage will undergo in acidic environments. Conditions were chosen to model a standard dilute acid pretreatment operating condition, but the conditions are also similar in temperature and acid loading to Organosolv-based processes such as Clean Fractionation.[33,52] Results clearly demonstrate that in acidic environments the presence of a phenolic-hydroxyl group accelerates the reaction rate of C−O bond cleavage in the β-O-4 linkage by 2 orders of magnitude. This dramatic rate increase is due to stabilization imparted to the key carbocation intermediate. Additionally, the presence of a methoxy group, which is commonly found in native lignin, blocks formation of a stable phenyl-dihydrobenzofuran compound.

Overall, these results help reconcile the disparity between studies examining lignin acidolysis in biomass,[12,34,35,58,92,93] which indicate at least partial aryl-ether bond cleavage on the time scale of minutes, and model compound studies[17,18,59,90,91] suggesting partial β-O-4 bond cleavage requires many hours. In biomass lignin, phenolic hydroxyl groups are typically found at termini of branched, heterogeneous lignin polymers. Thus, these results imply that lignin depolymerization during acidic pretreatment will proceed via an ionic, unzipping mechanism wherein β-O-4 linkages will be cleaved from the phenolic ends. This will likely continue along the polymer until bonds are reached that are much more recalcitrant to cleavage in acidic environments. Additionally, these results suggest that the presence of methoxy groups will affect the identity of the condensation products and will protect reaction intermediates from rapid self-condensation.

METHODS

Full synthetic and computational details are given in the Supporting Information (SI).

ASSOCIATED CONTENT

Supporting Information

Full synthesis and characterization of the compounds used in this study, complete description of the computational methods, and optimized Cartesian coordinates for all DFT calculations. This material is available free of charge via the Internet at http://pubs.acs.org.

AUTHOR INFORMATION

Corresponding Author

*E-mail: Gregg.beckham@nrel.gov.

Present Address

[¶]Center for Renewable Carbon, University of Tennessee Institute of Agriculture, Knoxville, TN USA.

Author Contributions

[⊥]These authors contributed equally.

Notes

The authors declare no competing financial interest.

ACKNOWLEDGMENTS

We acknowledge funding from the National Advanced Biofuels Consortium, which is funded by the DOE BioEnergy Technologies Office through American Recovery and Reinvestment Act Funds. R.S.P. thanks the Oxford University Press John Fell Fund and the Royal Society (RG RG110617) for funding. We acknowledge Marykate O'Brien, Jessica Hamlin, and Kellene McKinney for their help synthesizing model compounds, Luc Moens for his insightful mechanistic discussions, William Michener and Erica Gjersing for analysis, and J. D. McMillan for a critical reading of the manuscript. Computer time was provided by the Trestles and Gordon clusters at the San Diego Supercomputing Center and the Ember cluster at NCSA under the NSF XSEDE Grant MCB090159 and by the NREL Computational Sciences Center supported by the DOE Office of EERE under Contract Number DE-AC36-08GO28308.

REFERENCES

(1) Chundawat, S. P. S.; Beckham, G. T.; Himmel, M. E.; Dale, B. E. Deconstruction of lignocellulosic biomass to fuels and chemicals. *Annu. Rev. Chem. Biomol. Eng.* **2011**, *2*, 121−145.

(2) Lynd, L. R.; Laser, M. S.; Brandsby, D.; Dale, B. E.; Davison, B.; Hamilton, R.; Himmel, M.; Keller, M.; McMillan, J. D.; Sheehan, J.; Wyman, C. E. How biotech can transform biofuels. *Nat. Biotechnol.* **2008**, *26*, 169−172.

(3) Ragauskas, A. J.; Williams, C. K.; Davison, B. H.; Britovsek, G.; Cairney, J.; Eckert, C. A.; Frederick, W. J.; Hallett, J. P.; Leak, D. J.; Liotta, C. L.; Mielenz, J. R.; Murphy, R.; Templer, R.; Tschaplinski, T. The path forward for biofuels and biomaterials. *Science* **2006**, *311*, 484−489.

(4) Himmel, M. E.; Ding, S. Y.; Johnson, D. K.; Adney, W. S.; Nimlos, M. R.; Brady, J. W.; Foust, T. D. Biomass recalcitrance: Engineering plants and enzymes for biofuels production. *Science* **2007**, *315*, 804−807.

(5) Keasling, J. D.; Chou, H. Metabolic engineering delivers next-generation biofuels. *Nat. Biotechnol.* **2008**, *26*, 298−299.

(6) Peralta-Yahya, P. P.; Zhang, F. Z.; del Cardayre, S. B.; Keasling, J. D. Microbial engineering for the production of advanced biofuels. *Nature* **2012**, *488*, 320−328.

(7) Serrano-Ruiz, J. C.; Dumesic, J. A. Catalytic routes for the conversion of biomass into liquid hydrocarbon transportation fuels. *Energy Environ. Sci.* **2011**, *4*, 83−99.

(8) Bozell, J. J. Connecting biomass and petroleum processing with a chemical bridge. *Science* **2010**, *329*, 522−523.

(9) Bozell, J. J.; Petersen, G. R. Technology development for the production of biobased products from biorefinery carbohydrates-the US Department of Energy's "Top 10" revisited. *Green Chem.* **2010**, *12*, 539−554.
(10) Wyman, C. E.; Dale, B. E.; Elander, R. T.; Holtzapple, M.; Ladisch, M. R.; Lee, Y. Y. Coordinated development of leading biomass pretreatment technologies. *Bioresour. Technol.* **2005**, *96*, 1959−1966.
(11) Zakzeski, J.; Bruijnincx, P. C. A.; Jongerius, A. L.; Weckhuysen, B. M. The catalytic valorization of lignin for the production of renewable chemicals. *Chem. Rev.* **2010**, *110*, 3552−3599.
(12) Pu, Y.; Hu, F.; Huang, F.; Davison, B.; Ragauskas, A. Assessing the molecular structure basis for biomass recalcitrance during dilute acid and hydrothermal pretreatments. *Biotechnol. Biofuels* **2013**, *6*, 15.
(13) Boerjan, W.; Ralph, J.; Baucher, M. Lignin biosynthesis. *Annu. Rev. Plant Biol.* **2003**, *54*, 519−546.
(14) Vanholme, R.; Demedts, B.; Morreel, K.; Ralph, J.; Boerjan, W. Lignin biosynthesis and structure. *Plant Physiol.* **2010**, *153*, 895−905.
(15) Beste, A.; Buchanan, A. C. Computational study of bond dissociation enthalpies for lignin model compounds. Substituent effects in phenethyl phenyl ethers. *J. Org. Chem.* **2009**, *74*, 2837−2841.
(16) Beste, A.; Buchanan, A. C.; Harrison, R. J. Computational prediction of α/β selectivities in the pyrolysis of oxygen-substituted phenethyl phenyl ethers. *J. Phys. Chem. A* **2008**, *112*, 4982−4988.
(17) Yokoyama, T.; Matsumoto, Y. Revisiting the mechanism of β-O-4 bond cleavage during acidolysis of lignin. Part 1: Kinetics of the formation of enol ether from non-phenolic C-6−C-2 type model compounds. *Holzforschung* **2008**, *62*, 164−168.
(18) Yokoyama, T.; Matsumoto, Y. Revisiting the mechanism of β-O-4 bond cleavage during acidolysis of lignin. Part 2: Detailed reaction mechanism of a non-phenolic C-6−C-2 type model compound. *J. Wood Chem. Technol.* **2010**, *30*, 269−282.
(19) Westermark, U.; Samuelsson, B.; Lundquist, K. Homolytic cleavage of the β-ether bond in phenolic β-O-4 structures in wood lignin and in guaiacylglycerol-β-guaiacyl ether. *Res. Chem. Intermediat.* **1995**, *21*, 343−352.
(20) Roberts, V. M.; Stein, V.; Reiner, T.; Lemonidou, A.; Li, X. B.; Lercher, J. A. Towards quantitative catalytic lignin depolymerization. *Chem.—Eur. J.* **2011**, *17*, 5939−5948.
(21) Hicks, J. C. Advances in C−O bond transformations in lignin-derived compounds for biofuels production. *J. Phys. Chem. Lett.* **2011**, *2*, 2280−2287.
(22) Nichols, J. M.; Bishop, L. M.; Bergman, R. G.; Ellman, J. A. Catalytic C−O bond cleavage of 2-aryloxy-1-arylethanols and its application to the depolymerization of lignin-related polymers. *J. Am. Chem. Soc.* **2010**, *132*, 12554−12555.
(23) Wu, A.; Patrick, B. O.; Chung, E.; James, B. R. Hydrogenolysis of β-O-4 lignin model dimers by a ruthenium-xantphos catalyst. *Dalton Trans.* **2012**, *41*, 11093−11106.
(24) Wang, X. Y.; Rinaldi, R. Solvent effects on the hydrogenolysis of diphenyl ether with raney nickel and their implications for the conversion of lignin. *ChemSusChem* **2012**, *5*, 1455−1466.
(25) Desnoyer, A. N.; Fartel, B.; MacLeod, K. C.; Patrick, B. O.; Smith, K. M. Ambient-temperature carbon−oxygen bond cleavage of an α-aryloxy ketone with Cp_2Ti(BTMSA) and selective protonolysis of the resulting Ti−OR bonds. *Organometallics* **2012**, *31*, 7625−7628.
(26) Hanson, S. K.; Baker, R. T.; Gordon, J. C.; Scott, B. L.; Thorn, D. L. Aerobic oxidation of lignin models using a base metal vanadium catalyst. *Inorg. Chem.* **2010**, *49*, 5611−5618.
(27) Kelley, P.; Lin, S. B.; Edouard, G.; Day, M. W.; Agapie, T. Nickel-mediated hydrogenolysis of C−O bonds of aryl ethers: What is the source of the hydrogen? *J. Am. Chem. Soc.* **2012**, *134*, 5480−5483.
(28) Matson, T. D.; Barta, K.; Iretskii, A. V.; Ford, P. C. One-pot catalytic conversion of cellulose and of woody biomass solids to liquid fuels. *J. Am. Chem. Soc.* **2011**, *133*, 14090−14097.
(29) Rinaldi, R.; Schuth, F. Design of solid catalysts for the conversion of biomass. *Energy Environ. Sci.* **2009**, *2*, 610−626.
(30) Sergeev, A. G.; Hartwig, J. F. Selective, nickel-catalyzed hydrogenolysis of aryl ethers. *Science* **2011**, *332*, 439−443.
(31) Son, S.; Toste, F. D. Non-oxidative vanadium-catalyzed C-O bond cleavage: Application to degradation of lignin model compounds. *Angew. Chem., Int. Ed.* **2010**, *49*, 3791−3794.
(32) Tobisu, M.; Chatani, N. Catalytic hydrogenolysis of C−O bonds in aryl ethers. *ChemCatChem* **2011**, *3*, 1410−1411.
(33) Bozell, J. J.; O'Lenick, C. J.; Warwick, S. Biomass fractionation for the biorefinery: Heteronuclear multiple quantum coherence-nuclear magnetic resonance investigation of lignin isolated from solvent fractionation of switchgrass. *J. Agric. Food Chem.* **2011**, *59*, 9232−9242.
(34) Kobayashi, T.; Kohn, B.; Holmes, L.; Faulkner, R.; Davis, M.; Maciel, G. E. Molecular-level consequences of biomass pretreatment by dilute sulfuric acid at various temperatures. *Energy Fuels* **2011**, *25*, 1790−1797.
(35) Kohn, B.; Davis, M.; Maciel, G. E. *In situ* study of dilute H_2SO_4 pretreatment of C-13-enriched poplar wood, using C-13 NMR. *Energy Fuels* **2011**, *25*, 2301−2313.
(36) Lu, F. C.; Ralph, J. Solution-state NMR of lignocellulosic biomass. *J. Biobased Mater. Bio.* **2011**, *5*, 169−180.
(37) Mansfield, S. D.; Kim, H.; Lu, F. C.; Ralph, J. Whole plant cell wall characterization using solution-state 2D NMR. *Nat. Protoc.* **2012**, *7*, 1579−1589.
(38) Pu, Y. Q.; Cao, S. L.; Ragauskas, A. J. Application of quantitative P-31 NMR in biomass lignin and biofuel precursors characterization. *Energy Environ. Sci.* **2011**, *4*, 3154−3166.
(39) Donohoe, B. S.; Decker, S. R.; Tucker, M. P.; Himmel, M. E.; Vinzant, T. B. Visualizing lignin coalescence and migration through maize cell walls following thermochemical pretreatment. *Biotechnol. Bioeng.* **2008**, *101*, 913−925.
(40) Chundawat, S. P. S.; Donohoe, B. S.; Sousa, L. D.; Elder, T.; Agarwal, U. P.; Lu, F. C.; Ralph, J.; Himmel, M. E.; Balan, V.; Dale, B. E. Multi-scale visualization and characterization of lignocellulosic plant cell wall deconstruction during thermochemical pretreatment. *Energy Environ. Sci.* **2011**, *4*, 973−984.
(41) Mosier, N.; Wyman, C.; Dale, B.; Elander, R.; Lee, Y. Y.; Holtzapple, M.; Ladisch, M. Features of promising technologies for pretreatment of lignocellulosic biomass. *Bioresour. Technol.* **2005**, *96*, 673−686.
(42) Chen, F.; Dixon, R. A. Lignin modification improves fermentable sugar yields for biofuel production. *Nat. Biotechnol.* **2007**, *25*, 759−761.
(43) Fu, C. X.; Mielenz, J. R.; Xiao, X. R.; Ge, Y. X.; Hamilton, C. Y.; Rodriguez, M.; Chen, F.; Foston, M.; Ragauskas, A.; Bouton, J.; Dixon, R. A.; Wang, Z. Y. Genetic manipulation of lignin reduces recalcitrance and improves ethanol production from switchgrass. *Proc. Natl. Acad. Sci. U.S.A.* **2011**, *108*, 3803−3808.
(44) Ziebell, A.; Gracom, K.; Katahira, R.; Chen, F.; Pu, Y. Q.; Ragauskas, A.; Dixon, R. A.; Davis, M. Increase in 4-coumaryl alcohol units during lignification in alfalfa (medicago sativa) alters the extractability and molecular weight of lignin. *J. Biol. Chem.* **2010**, *285*, 38961−38968.
(45) Carpita, N. C. Progress in the biological synthesis of the plant cell wall: new ideas for improving biomass for bioenergy. *Curr. Opin. Biotechnol.* **2012**, *23*, 330−337.
(46) McCann, M. C.; Carpita, N. C. Designing the deconstruction of plant cell walls. *Curr. Opin. Plant Biol.* **2008**, *11*, 314−320.
(47) Simmons, B. A.; Logue, D.; Ralph, J. Advances in modifying lignin for enhanced biofuel production. *Curr. Opin. Plant Biol.* **2010**, *13*, 313−320.
(48) Li, X.; Weng, J. K.; Chapple, C. Improvement of biomass through lignin modification. *Plant J.* **2008**, *54*, 569−581.
(49) Humphreys, J. M.; Chapple, C. Rewriting the lignin roadmap. *Curr. Opin. Plant Biol.* **2002**, *5*, 224−229.
(50) Bonawitz, N. D.; Chapple, C. The genetics of lignin biosynthesis: Connecting genotype to phenotype. *Annu. Rev. Genet.* **2010**, *44*, 337−363.
(51) Weng, J. K.; Li, X.; Bonawitz, N. D.; Chapple, C. Emerging strategies of lignin engineering and degradation for cellulosic biofuel production. *Curr. Opin. Biotechnol.* **2008**, *19*, 166−172.

(52) Bozell, J. J.; Black, S. K.; Myers, M.; Cahill, D.; Miller, W. P.; Park, S. Solvent fractionation of renewable woody feedstocks: Organosolv generation of biorefinery process streams for the production of biobased chemicals. *Biomass Bioenerg.* **2011**, *35*, 4197−4208.
(53) Zhang, Y. H. P.; Ding, S. Y.; Mielenz, J. R.; Cui, J. B.; Elander, R. T.; Laser, M.; Himmel, M. E.; McMillan, J. R.; Lynd, L. R. Fractionating recalcitrant lignocellulose at modest reaction conditions. *Biotechnol. Bioeng.* **2007**, *97*, 214−223.
(54) Fort, D. A.; Remsing, R. C.; Swatloski, R. P.; Moyna, P.; Moyna, G.; Rogers, R. D. Can ionic liquids dissolve wood? Processing and analysis of lignocellulosic materials with 1-*n*-butyl-3-methylimidazolium chloride. *Green Chem.* **2007**, *9*, 63−69.
(55) Pu, Y. Q.; Jiang, N.; Ragauskas, A. J. Ionic liquid as a green solvent for lignin. *J. Wood Chem. Technol.* **2007**, *27*, 23−33.
(56) Li, C. L.; Knierim, B.; Manisseri, C.; Arora, R.; Scheller, H. V.; Auer, M.; Vogel, K. P.; Simmons, B. A.; Singh, S. Comparison of dilute acid and ionic liquid pretreatment of switchgrass: Biomass recalcitrance, delignification and enzymatic saccharification. *Bioresour. Technol.* **2010**, *101*, 4900−4906.
(57) Moxley, G.; Gaspar, A. R.; Higgins, D.; Xu, H. Structural changes of corn stover lignin during acid pretreatment. *J. Ind. Microbiol. Biot.* **2012**, *39*, 1289−1299.
(58) Cao, S. L.; Pu, Y. Q.; Studer, M.; Wyman, C.; Ragauskas, A. J. Chemical transformations of populus trichocarpa during dilute acid pretreatment. *RSC Advances* **2012**, *2*, 10925−10936.
(59) Ito, H.; Imai, T.; Lundquist, K.; Yokoyama, T.; Matsumoto, Y. Revisiting the mechanism of β-O-4 bond cleavage during acidolysis of lignin. Part 3: Search for the rate-determining step of a non-phenolic C-6−C-3 type model compound. *J. Wood Chem. Technol.* **2011**, *31*, 172−182.
(60) Lundquist, K. Acid degradation of lignin. 8. Low-molecular weight phenols from acidolysis of birch lignin. *Acta Chem. Scand.* **1973**, *27*, 2597−2606.
(61) Li, S. M.; Lundquist, K.; Westermark, U. Cleavage of arylglycerol beta-aryl others under neutral and acid conditions. *Nord. Pulp Pap. Res. J.* **2000**, *15*, 292−299.
(62) Lundquist, K. Acid degradation of lignin. 2. Separation and identification of low molecular weight phenols. *Acta Chem. Scand.* **1970**, *24*, 889−907.
(63) Lundquist, K.; Ericsson, L. Acid degradation of lignin. 3. Formation of formaldehyde. *Acta Chem. Scand.* **1970**, *24*, 3681−3686.
(64) Lundquist, K.; Ericsson, L. Acid degradation of lignin. 6. Formation of methanol. *Acta Chem. Scand.* **1971**, *25*, 756−758.
(65) Lundquist, K.; Hedlund, K. Acid degradation of lignin. 5. Degradation products related to phenylcoumaran type of structure. *Acta Chem. Scand.* **1971**, *25*, 2199−2210.
(66) Lundquist, K.; Kirk, T. K. Acid degradation of lignin. 4. Analysis of lignin acidolysis products by gas chromatography, using trimethylsilyl derivatives. *Acta Chem. Scand.* **1971**, *25*, 889−894.
(67) Lundquist, K.; Lundgren, R. Acid degradation of lignin. 7. Cleavage of ether bonds. *Acta Chem. Scand.* **1972**, *26*, 2005−2023.
(68) Yasuda, S.; Terashima, N.; Ito, T. Chemical structures of sulfuric acid lignin IV. Reaction of arylglycerol-β-aryl ether with 72% sulfuric acid. *Mokuzai Gakkaishi* **1981**, *27*, 879−884.
(69) Yasuda, S.; Terashima, N.; Ito, T. Chemical structures of sulfuric acid lignin. I. Chemical structures of condensation products from monolignols. *Mokuzai Gakkaishi* **1980**, *26*, 552−557.
(70) Yasuda, S.; Terashima, N.; Ito, T. Chemical structures of sulfuric acid lignin. II. Chemical structures of condensation products from arylglycerol-β-aryl ether type structures. *Mokuzai Gakkaishi* **1981**, *27*, 216−222.
(71) Ito, T.; Terashima, N.; Yasuda, S. Chemical structures of sulfuric acid lignin. III. Reaction of arylglycerol-β-aryl ether with 5% sulfuric acid. *Mokuzai Gakkaishi* **1981**, *27*, 484−490.
(72) Yasuda, S.; Ota, K. Chemical structures of sulfuric acid lignin. IX. Reaction of syringyl alcohol and reactivity of guaiacyl and syringyl nuclei in sulfuric acid solution. *Mokuzai Gakkaishi* **1986**, *32*, 51−58.
(73) Yasuda, S.; Ota, K. Chemical structures of sulfuric acid lignin. Part X. Reaction of syringylglycerol-β-syringyl ether and condensation of syringyl nucleus with guaiacyl lignin model compounds in sulfuric acid. *Holzforschung* **1987**, *41*, 59−65.
(74) Yasuda, S.; Murase, N. Chemical structures of sulfuric acid lignin. Part XII. Reaction of lignin models with carbohydrates in 72% H_2SO_4. *Holzforschung* **1995**, *49*, 418−422.
(75) Yasuda, S.; Terashima, N. Chemical structures of sulfuric acid lignin. V. Reaction of three arylglycerol-β-aryl ethers [α-, β-, and γ-13C] with 72% sulfuric acid. *Mokuzai Gakkaishi* **1982**, *28*, 383−387.
(76) Yasuda, S.; Terashima, N.; Hamanaka, A. Chemical structures of sulfuric acid lignin. VI. Physical and chemical properties of sulfuric acid lignin. *Mokuzai Gakkaishi* **1983**, *29*, 795−800.
(77) Yasuda, S. Chemical structures of sulfuric acid lignin. VII. Reaction of phenylcoumaran with sulfuric acid. *Mokuzai Gakkaishi* **1984**, *30*, 166−172.
(78) Yasuda, S.; Adachi, K.; Terashima, N.; Ota, K. Chemical structures of sulfuric acid lignin. VIII. Reactions of 1,2-diaryl-1,3-propanediol and pinoresinol with sulfuric acid. *Mokuzai Gakkaishi* **1985**, *31*, 125−131.
(79) Yasuda, S.; Hirano, J. Chemical structures of sulfuric acid lignin. XI. Physical and chemical properties of beech sulfuric acid lignin. *Mokuzai Gakkaishi* **1990**, *36*, 454−459.
(80) Yasuda, S.; Ota, K. Chemical structures of sulfuric-acid lignin. 10. Reaction of syringylglycerol-β-syringyl ether and condensation of syringyl nucleus with guaiacyl lignin model compounds in sulfuric acid. *Holzforschung* **1987**, *41*, 59−65.
(81) Li, S.; Lundquist, K. Reactions of the β-aryl ether lignin model 1-(4-hydroxy-3-methoxyphenyl)-2-(2-methoxyphenoxy)-1-propanol on heating in aqueous solution. *Holzforschung* **2001**, *55*, 296−301.
(82) Sano, Y. Hydrolysis of lignin with dioxane-water. XV. Hydrolysis of 1-guaiacyl-2-quaiacoxy-1-propane-3-ol and guaiacylglycerol-b-gauiacyl ether. *Mokuzai Gakkaishi* **1975**, *21*, 508−519.
(83) Sano, Y.; Endo, S.; Sakakibara, A. Hydrolysis of lignin with dioxane-water. Hydrolysis of some model compounds (3). *Mokuzai Gakkaishi* **1977**, *23*, 193−198.
(84) Xu, H.; Omori, S.; Lai, Y. The alkaline stability of α-5 diphenylmethane dimers. *Holzforschung* **1995**, *49*, 323−324.
(85) Nimz, H. A new type of rearrangement in the lignin field. *Angew. Chem., Int. Ed. Engl.* **1966**, *5*, 843.
(86) Omori, S.; Aoyama, M.; Sakakibara, A. Hydrolysis of lignin with dioxane-water XIX. Reaction of β-O-4 lignin model compounds in the presence of carbohydrates. *Holzforschung* **1998**, *52*, 391−397.
(87) Kim, S.; Chmely, S. C.; Nimos, M. R.; Bomble, Y. J.; Foust, T. D.; Paton, R. S.; Beckham, G. T. Computational study of bond dissociation enthalpies for a large range of native and modified lignins. *J. Phys. Chem. Lett.* **2011**, *2*, 2846−2852.
(88) Beste, A.; Buchanan, A. C. Kinetic analysis of the phenyl-shift reaction in beta-O-4 lignin model compounds: A computational study. *J. Org. Chem.* **2011**, *76*, 2195−2203.
(89) Parthasarathi, R.; Romero, R. A.; Redondo, A.; Gnanakaran, S. Theoretical study of the remarkably diverse linkages in lignin. *J. Phys. Chem. Lett.* **2011**, *2*, 2660−2666.
(90) Imai, T.; Yokoyama, T.; Matsumoto, Y. Revisiting the mechanism of β-O-4 bond cleavage during acidolysis of lignin IV: Dependence of acidolysis reaction on the type of acid. *J. Wood Sci.* **2011**, *57*, 219−225.
(91) Imai, T.; Yokoyama, T.; Matsumoto, Y. Revisiting the mechanism of β-O-4 bond cleavage during acidolysis of lignin: Part 5: On the characteristics of acidolysis using hydrobromic acid. *J. Wood Chem. Technol.* **2012**, *32*, 165−174.
(92) Hu, G.; Cateto, C.; Pu, Y. Q.; Samuel, R.; Ragauskas, A. J. Structural characterization of switchgrass lignin after ethanol organosolv pretreatment. *Energy Fuels* **2012**, *26*, 740−745.
(93) Samuel, R.; Foston, M.; Jiang, N.; Allison, L.; Ragauskas, A. J. Structural changes in switchgrass lignin and hemicelluloses during pretreatments by NMR analysis. *Polym. Degrad. Stab.* **2011**, *96*, 2002−2009.

(94) Hauteville, M.; Lundquist, K.; Vonunge, S. NMR-studies of lignins. 7. H-1-NMR spectroscopic investigation of the distribution of erythro and threo forms of β-O-4 structures in lignins. *Acta. Chem. Scand. Ser. B-Org. Chem. Biochem.* **1986**, *40*, 31−35.
(95) Lai, Y.-Z. Chemical degradation. *Wood Cellul. Chem.* **2001**, *2*, 443−512.